Chemistry–A European Journal
Research Article
doi.org/10.1002/chem.202400442
Chemistry Europe
European Chemical Societies Publishing
www.chemeurj.org

AuNP/MIL-88B-NH_2 Nanocomposite for the Valorization of Nitroarene by Green Catalytic Hydrogenation

Sorraya N. K. Lelouche,[a, b] Ignacio Lemir,[a] Catalina Biglione,[a] Tim Craig,[c] Sara Bals,[c] and Patricia Horcajada*[a]

The efficiency of a catalytic process is assessed based on conversion, yield, and time effectiveness. However, these parameters are insufficient for evaluating environmentally sustainable research. As the world is urged to shift towards green catalysis, additional factors such as reaction media, raw material availability, sustainability, waste minimization and catalyst biosafety, need to be considered to accurately determine the efficacy and sustainability of the process. By combining the high porosity and versatility of metal organic frameworks (MOFs) and the activity of gold nanoparticles (AuNPs), efficient, cyclable and biosafe composite catalysts can be achieved. Thus, a composite based on AuNPs and the nanometric flexible porous iron(III) aminoterephthalate MIL-88B-NH_2 was successfully synthesized and fully characterized. This nanocomposite was tested as catalyst in the reduction of nitroarenes, which were identified as anthropogenic water pollutants, reaching cyclable high conversion rates at short times for different nitroarenes. Both synthesis and catalytic reactions were performed using green conditions, and even further tested in a time-optimizing one-pot synthesis and catalysis experiment. The sustainability and environmental impact of the catalytic conditions were assessed by green metrics. Thus, this study provides an easily implementable synthesis, and efficient catalysis, while minimizing the environmental and health impact of the process.

Introduction

Many reactions require at least one catalytic step, typically describing their efficiency by its conversion, yield and time efficacy.[1,2] However, these parameters are insufficient when targeting environmentally sustainable research.[3,4] Furthermore, as the world is moving away from resource driven catalysis and towards green catalysis, more factors are needed to properly evaluate the efficacy and sustainability of the catalytic processes.[5–8] Indeed, green catalysis must additionally consider parameters such as the reaction media, the availability and the sustainability of the raw material as well as, the environmental impact of the catalysts.[9–11] Thus, several green metrics were created in order to compare the sustainability and/or environmental impact of a chemical process.[12,13] Herein, a semi quantitative method based on the 12 principles of green chemistry was used to represent the greenness of the reaction; the green star and mass metrics were used to compare this work to others.[14]

The field of catalysis ranges over a broad spectrum of applications, among which is the valorization of toxic compounds. Indeed, the increasing presence of organic contaminants in the environment is one of the most significant concerns today.[15] Nitroarenes are widely renown as mutagenic, cytotoxic, carcinogenic and potentially explosive.[16,17] One of the main challenges in removing these contaminants is their high aqueous solubility and significant redox stability, owing to their well-known electron-accepting nature.[18] This is why various methodologies have been proposed for removing them, based mainly redox, photo-Fenton, and denaturation processes.[19] The current trend focuses on the reduction of the nitro group into anilines as they are compounds of great industrial value and important chemical precursors.[20] Consequently, studying the formation of anilines from contaminants is of great interest to the scientific community as well as for the society.

Focusing on the reduction of nitroaromatics to anilines, various metal nanoparticles (NPs; *i.e.* Pt, Pd, Ag, Au, Co, Ni, Cu) have demonstrated a relevant catalytic activity, with high performance and yield.[18,21] Moreover, using metal NPs as heterogeneous catalysts allows an easy catalyst removal, avoiding purification steps, potential reuse, and extension of the lifespan. Several of the aforementioned metals raise safety issues.[22] In particular, Pd is one of the most active metals for hydrogenation. However, several Pd salts are cytotoxic, and as

[a] S. N. K. Lelouche, Dr. I. Lemir, Dr. C. Biglione, Dr. P. Horcajada
Advanced Porous Materials Unit (APMU)
IMDEA Energy Institute
Av. Ramón de La Sagra, 3, 28935, Móstoles, Madrid, Spain
E-mail: patricia.horcajada@imdea.org
[b] S. N. K. Lelouche
EID
University Rey Juan Carlos (URJC)
Tulipán s/n,
Móstoles, 28933, Spain
[c] T. Craig, Prof. S. Bals
EMAT and NANOlab Center of Excellence
University of Antwerp
Groenenborgerlaan 171
Antwerp, 2020, Belgium

Supporting information for this article is available on the WWW under https://doi.org/10.1002/chem.202400442

such present a risk to the operator.[23] In contrast gold, is biocompatible[24] and gold nanoparticles (AuNPs) are excellent catalysts in hydrogenation,[25] H_2 formation,[26] or polymerization reactions[27] due to their exceptional properties (optoelectronic, biocompatibility, tunable size, shape and surface).[28] However, AuNPs possess a limited stability (by sintering) and high cost.[29] By immobilizing the NPs on a support, these issues can be overcome, improving the catalyst stability and cyclability.[30] Although most frequent supports present no intrinsic activity (metal oxides, polymers),[31,32] synergistic catalytic properties could be obtained by using active solid supports. In this line, metal organic frameworks (MOFs), composed of inorganic nodes bridged by organic linkers,[33] offer broad possibilities: i) their great structural/compositional diversity is favorable for numerous catalytic routes,[1,33,34] ii) their exceptional porosity might provide a confinement effect, wear protection and/or selectivity,[35] and iii) the vast collection of MOFs allows selecting environmentally friendly and biosafe material.

Particularly, a few AuNP/MOF catalysts have been reported for the reduction of nitroarenes using different micro- and nano-scaled MOFs (nanoMIL-100(Fe),[36] nanoMIL-125(Ti),[37] and Cu(II)-MOF,[38]). Indeed, nanosized MOFs have proven enhanced catalytic results compared to micro-sized particles.[39] Reaction conditions involve $NaBH_4$ as a reducing agent and short reaction times. Nevertheless, these methodologies require an excess of reducing agent and so far, the exploration of nitroarene compounds to be reduced is very limited. The optimal results achievable with these gold composites demonstrated an apparent synergistic effect: AuNPs play the role of the active phase where the catalytic phenomenon (substrate-metal interaction) occurs, whereas the MOF assists in stabilizing and enhancing the catalytic and colloidal properties.[40] Further, Au@nanoMIL-101(Fe)–NH_2 has been very recently used for the hydrogenation of 4-nitrophenol,[41] showing a high conversion to 4-aminophenol in only 20 seconds. This cubic MOF, with a highly rigid porosity (Brunauer-Emmett-Teller surface (S_{BET}) ~2300 $m^2.g^{-1}$ and pore sizes of ~3.0 & 3.4 nm, accessible *via* microporous windows 1.2 & 1.5 nm), is environmentally friendly and biosafe.[42,43] Furthermore, its polymorph MIL-88B-NH_2 also presents a high but flexible porosity (theoretical S_{BET} ~2040 $m^2.g^{-1}$ and pore size ~1.5 nm in the open form) able to reversibly change its opening as a consequence of different external stimuli (*e.g.* adsorbate, pressure; from unit cell volumes of 1510 Å in the empty-close structure to up to 3430 Å in the ethanol-open form without any bonding breaking).[44,45] This exceptional "breathing" effect of the framework opens up the possibility of steric selectivity for both adsorption and catalytic processes. This remarkable property, along with its environmentally friendly composition[43] and high stability make MIL-88B-NH_2 a promising MOF for the stabilization of biosafe AuNPs and catalytic applications. Despite their interest, no flexible MOFs have been proposed for the reduction of nitroarenes up to now. In this sense, a novel AuNP/MIL-88B-NH_2 composite, was here successfully synthesized, fully characterized and used for the reduction of nitroarenes with encouraging results, which was assessed by green metrics. The focal difference between this work and previously reported ones, does not lay in the methodology, but in the fact that the synthesis is simple, robust and highly reproducible, disregarding several factors (e.g. temperature changes, interbatches, operators). Lastly, the use of green metrics aims at emphasizing the impact of current materials.

Results and Discussion

Synthesis Optimization

MOF based composites can be synthesized mainly by three methods: -core-shell; -impregnation; and -in situ *NP growth*.[46] The latter was here selected because it presents some advantages: i) it allows a higher loading of AuNPs, which constitute the active component of the catalyst;[47] ii) AuNPs are protected within the MOF; and iii) it offers an easier scale-up than the core-shell strategy.[48] Thus, the composite was here obtained by *in-situ* NP growth, initially synthesizing the MOF (stabilizing matrix), inserting the gold ions ($HAuCl_4$) then by impregnation and, finally, reducing the metal ions into metal NPs inside the matrix. Chemical reduction was here selected as it does not require specific equipment, unlike sono- and photo-reduction, as such it is easily achievable. $NaBH_4$ was chosen as the reducing agent since it is cost efficient, readily available and highly efficient. Three main parameters were screened (Table S1): the impregnation time of the gold solution, the Au/MOF ratio and the ratio of MOF/$NaBH_4$, while the quantity of MOF was kept constant. Except for the highest MOF/$NaBH_4$ ratio with some structural changes, the crystallinity of the MOF was kept intact upon the AuNP formation (see Powder X-Ray Diffraction-PXRD in Figure S1). Furthermore, the MOF chemical integrity was confirmed by a very low linker release (< 3 %; Table S2), observing an effect of the MOF/$NaBH_4$ ratio as the highest amount of the reducing agent leads to the highest MOF degradation (linker release = 6.4 %). The linker release was quantified by High-Performance Liquid Chromatography (HPLC), by collecting and analyzing the supernatant after centrifugation at the end of the synthesis (see experimental section for more details). When looking into the size of the formed AuNPs, it appears that with a higher gold content and $NaBH_4$, the obtained AuNPs are larger and seem mainly located on the MOF outer surface (see Transmission Electron Microscopy or "TEM" images in Figure S2 and Table S2). Furthermore, the size and location of the NP are very heterogeneous. In contrast, the lowest quantity of gold and $NaBH_4$ with shorter times led to the most homogeneous distribution of AuNPs embedded in the MOF matrix. Therefore, the best tested synthesis conditions for the composite were: MIL-88B-NH_2 and gold dispersed in MilliQ at a MOF/Au ratio of 0.78. After 4 h stirring, the gold excess was removed by centrifugation. The material was then redispersed in water and $NaBH_4$ in methanol was added dropwise, at a MOF/$NaBH_4$ ratio of 0.003. It is important to highlight that this method provides a straight forward, and highly reproducible synthesis (performed by different operators, and at different period of the year).

Characterization of AuNP/MIL-88B-NH_2 Nanocomposite

The composite obtained via the best tested condition, was fully characterized by different techniques. First, the pure crystal structure corresponding to the water-open form of MIL-88B-NH_2 (~2040 Å)[49] was confirmed for the composite by PXRD (Figure 1), observing no detrimental effect on the MOF's crystallinity by the *in situ* AuNPs formation. Furthermore, the characteristic peaks of the face centered cubic (FCC) structure of gold can be observed at higher angle (37.5 and 44.5° 2θ), confirming the presence of crystalline gold, broadening of these peaks is coherent with the presence of AuNPs.[50] Lastly, the crystallinity index of the material was calculated, by dividing the integrated area of the crystalline peaks by that of the entire diffractogram as a whole.[51] The materials have a crystallinity index of 97% for the pristine MOF and 95% for the composite. These high indices prove the high crystallinity of the materials.

The integrity of the MOF structure was also confirmed by the lower linker release (only 3.2±0.9% of linker was detected over the entire synthesis). In addition, Fourier Transform-infrared (FT-IR) spectra (Figure S3) show no indication of free carboxylic acid at ~1700 cm^{-1}, proving that no free linker is trapped within the structure and that the free linker quantified by High Performance Liquid Chromatography (HPLC) accurately describes the process. Moreover, the band at 1095 cm^{-1}, characteristic of N–H vibrations, is barely notable in the MOF but well-defined in the composite.[52] This could be explained by the polarization of the N–H bond due to the presence of the gold,[53] inferring that the gold is collocated with the amine group and therefore, in the porosity. Note here that the porosity of MIL-88B-NH2 is not accessible to N2 sorption since the structure remains close upon outgassing, when dehydrated. The data extracted from the PXRD, HPLC and FTIR emphasize the purity of the obtained materials.

In an attempt to more precisely localize the AuNPs and further describe the morphology of the composite, TEM and Scanning TEM (STEM) images were collected. High angle annular dark field STEM micrographs (Figure 2) show the typical hexagonal needle shaped MOF particles of MIL-88B-NH_2, with an approximate aspect ratio of 300×80 nm. Upon the formation of AuNPs, both the morphology and size of the MOF is maintained (Figure 2 and S4). Moreover, small denser particles, corresponding to the AuNPs, can be observed homogeneously dispersed throughout the sample and within the MOF, with a diameter of 2.7±0.9 nm the AuNP were measured from the images in Figure 2, excluding the ones seemingly located at the surface (Figure S5A). Elemental mapping (Energy-Dispersive X-Ray Spectroscopy, EDS) was performed (Figure S5B–C), confirming the identification of AuNPs with a ratio Au/Fe of 0.1. To locate the AuNPs more precisely, electron tomography was performed and the result is illustrated in Video S1–2. Although some AuNPs are visible on the MOF outer surface, the overall results cement that AuNPs are mainly located inside the MOF network/porosity.

The size of the material was measured in aqueous solution and ethanol using Dynamic Light Scattering (DLS), see Figure S6A. DLS has limitations, it is meant for spherical particles, as such the technique is not optimal for the characterization of elongated particles. Nevertheless, it can be used to see a tendency towards aggregation of colloidal dispersions in different media. The hydrodynamic size of the MOF and the composite showed no significant change in ethanol, exhibiting a particle size fully in agreement with the TEM observations (~250 nm; Figure S6A). However, the composite exhibits a higher polydispersity index (PDI), which is potentially associated with an aggregation tendency. In addition, (Figure S6B) an inversion in the zeta potential can be noted after the *in situ*

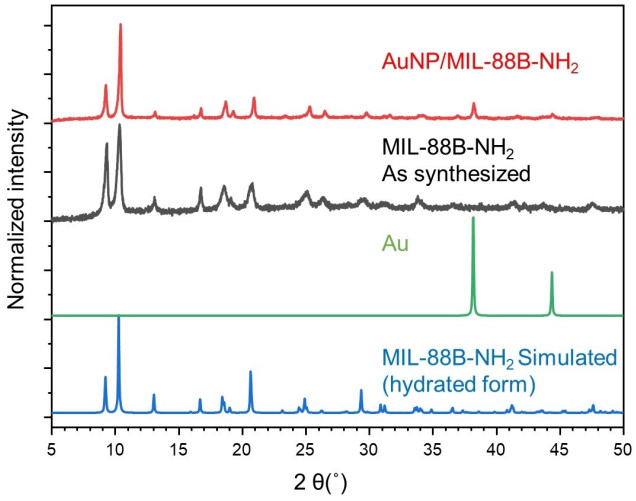

Figure 1. PXRD patterns of AuNP/MIL-88B-NH_2, and MIL-88B-NH_2, as well as the simulated patterns of gold and MIL-88B-NH_2 in the hydrated form.

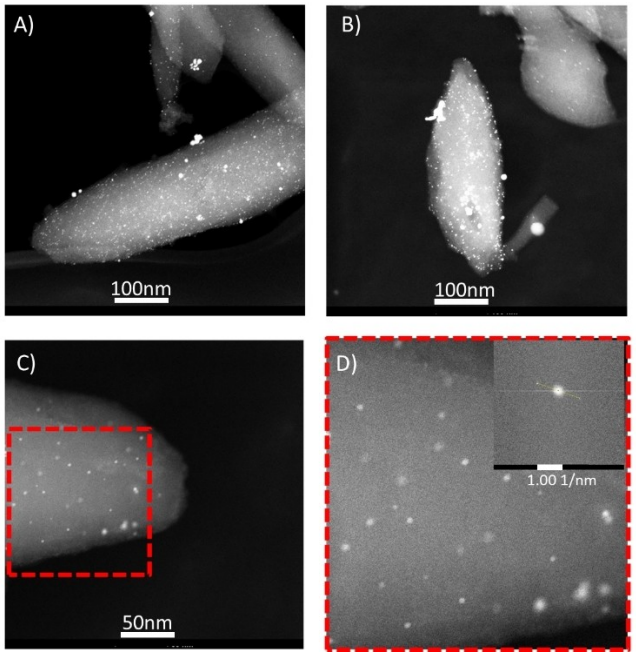

Figure 2. HAADF-STEM images of AuNP/MIL-88B-NH_2 showing the needle-like morphology (A–B). HAADF-STEM imaging of the tip of an AuNP/MIL-88B-NH_2 needle show imbedded AuNPs throughout the MOF (C). The red box shows a region of the AuNP/MIL-88B-NH_2 which was rescaled for improved visualization. The inset is the fast Fourier transform of the image (D).

formation of AuNPs (45 ± 17 mV, in accordance with reported values,[54] *vs.* −20 ± 3 mV). This drastic change could be explained by the presence of AuNPs on the surface of the MOF.[55,56] Despite the similar surface charge in water for both the MOF and the composite, larger dimensions are observed in water (~650 nm), which might also be related to the aggregation in water.

Considering the potential light absorption of AuNPs, UV-Vis spectra were collected (Figure S7). Both materials absorb at 380 nm; this signal arising from the MOF's constitutive linker, the 2-aminoterephthalate. In addition, the composite's spectrum showed a shoulder at around 570 nm, which may be caused by the presence of AuNPs. The absorbance wavelength of single AuNPs can be correlated to its size and shape.[57–59] Nevertheless, small nanoparticles, like here tend to have weak signal and are hard to detect. Moreover, when the particles are coated with a polymer or imbedded in a matrix (like here the MOF), the absorbance of the AuNPs can greatly vary, and be dampened by surface interactions.[60] Indeed, because the absorbance of AuNP are due to the oscillation of surface electrons, interactions and bonds between them and the MOF greatly alter their absorption. Here, the signal of the AuNP is dampened presumably because they are mainly buried inside of the MOF and are in all likelihood interacting with it through weak surface interactions.[61,62] Therefore, it was not possible to accurately confirm the size of the AuNPs in the composite solely based on the UV-visible spectra.

To estimate the gold content in the sample, Thermogravimetric Analysis (TGA) was performed (Figure S8A). The composite and the bare nanoMOF experience a first weight loss at around 90 °C (10 and 13 wt.%, respectively), which is due to the evaporation of adsorbed solvents (*i.e.*, ethanol and water). Until 200 °C, a slow weight loss occurs due to the elimination of water molecules coordinated to the iron metal sites of MIL-88B-NH_2 (6 and 8 wt.%, respectively). The main degradation step occurs between 200 and 400 °C when the linker combustion happens. On the one hand, for the bared MOF, the linker degrades in one steep step (53 wt.%), leaving 29% of Fe_2O_3 residue (as confirmed by XRD).[63] On the other hand, the composite's linker degradation occurs in 3 sub-steps (adding to a weight loss of 55%, and a residue 35% of Fe_2O_3 and 2% of Au). One could hypothesize that the sub-steps are related with different interactions between the linker and the AuNPs. The first step (200–280 °C, 78% of the total ligand) could correspond to the degradation of the linker with no direct interaction with the AuNPs. Between 280 and 380 °C, could be associated with the linker in weak interaction with AuNPs (16% the total linker). And the last small step, between 380 and 400 °C, might be the remaining 5% ligand directly interacting with the AuNPs. The iron and gold content were calculated from the TGA data, as well as from Inductively Coupled Plasma Optical Emission Spectroscopy (ICP-OES; Figure S8B), resulting in 19.6 ± 1.0% and 18.5 ± 1.2% of Fe for the bare MOF and 20.6 ± 1.0% and for the composite, 23.1 ± 1.5% of Fe and 1.9 ± 0.1% and 1.6 ± 0.4% of Au, by ICP and TGA, respectively. The results of the two methods are in good accordance and Au loading can be calculated, finding that the MOF is loaded with 1.6 wt% of gold This corresponds to a ratio Au/Fe of 0.08 which is in agreement to the EDS results (ratio of Au/Fe 0.1).

Catalytic Reduction of Nitroarenes

With the final aim to reduce and valorize the anthropogenic water pollutants nitroarenes, we propose here the reduction of nitrobenzene to aniline using the AuNP/MIL-88B-NH_2 composite as catalyst (Table 1). Our primary objective is to design an environmentally friendly strategy, employing non-hazardous solvents (*i.e.* water, ethanol) at room temperature and sustainable hydrogen sources such as $NaBH_4$. The optimization of the reaction conditions (solvent, time, amount of $NaBH_4$) is detailed in Table 1. Initially, water was tested as solvent; but the catalysis was ineffective due to the hydrophobic nature of compound **1a** (solubility in water at 20 °C = 0.2 mg·mL^{-1}),[64] hindering the proper reaction mixture (entry 1). Additionally, it is well-known that a minimum amount of alcohol is required to activate the $NaBH_4$, performing as a reducing agent or hydrogen donor. Following this, ethanol was employed as solvent, achieving a 100% conversion and 99% yield (entry 2). It is worth noting that by using aqueous mixtures of water and ethanol, the reaction remains effective, reaching complete conversions in a water/ethanol ratio of 70:30. This is important because the alcohol not only activates the reducing agent but also facilitates the substrate dissolution in the reaction medium, leading to an improvement in the conversion (entries 3, 4 & 5). In order to assess the colloidal stability of the material in the catalytic conditions, DLS measurements were performed at different ratios of ethanol/water, (Figure S9). The use of a water ethanol mixture is crucial for the reduction of nitro groups in more complex organic molecules, as it favors their solubility. The results indicate that the material is more colloidally stable in ethanol. Furthermore, the data indicates no significant changes in the different solvent mixtures and pure water. As such the analysis shows that the colloidal stability does not determine the yield changes in the different solvent mixtures. Moreover, the chemical and structural stability of the material in these mixtures over 16 h at the concentration used in catalysis (5 mg.mL^{-1}) were tested (Figure S10). The results show that the crystalline structure is maintained as proved by PXRD, and the linker release is minimal (maximum linker release was = 1.67%). These stability test show that the material is particularly robust under the tested operating conditions. Continuing with the optimization of reaction parameters, we reduced the time significantly, from the initial 3 hours to just 30 minutes, without severely affecting the conversion (entries 6 & 7). Finally, reducing the amount of $NaBH_4$ is an interesting aspect to comply with the principles of green chemistry and atomic economy. In this case, the usage of the reducing agent was halved (entry 8), but decreasing it further resulted in a decreased conversion (entry 9).

After determining the optimal reaction conditions, the essential requirement for using a catalyst in the formation of **2a** becomes evident, as highlighted in absence of catalyst (entry 10). Subsequently, the bared MOF was tested in the absence

Table 1. Reduction of nitrobenzene to aniline.

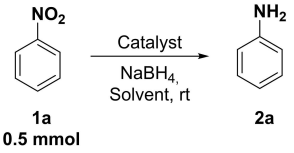

Entry	Solvents	Catalyst	Time (h)	$NaBH_4$ (equiv)	Conversion	TOF
1	H_2O	**AuNP/MIL-88B-NH_2**	3	3	n.r.	0
2	EtOH		3	3	>99%	205
3	H_2O:EtOH (50:50)		3	3	52%	107
4	H_2O:EtOH (80:20)		3	3	74%	152
5	**H_2O:EtOH (70:30)**		3	3	>99%	205
6			2	3	>99%	308
7			**0.5**	3	>99%	1231
8				**1.5**	**88%**	**1083**
9				0.5	22%	281
10		No catalyst		1.5	n.r.	0
11		MIL-88B-NH_2		1.5	n.r.	0
12		AuNPs	0.5	1.5	n.r.	0

Reaction conditions: 1a (0.5 mmol), solvent (2 mL) and 10 mg of Au/MIL-88B-NH_2 at room temperature under magnetic stirring. Conversions were obtained by Gas Chromatography-Mass Spectrometry (GC-MS) using relative areas TOF (turnover frequency, h^{-1}) = moles of product/ (moles of catalyst x time). n.r. stands for no reaction.

of the AuNPs, demonstrating the lack of catalytic properties of MIL-88B-NH_2 for the targeted hydrogenation reaction (entry 11). Finally, AuNPs of similar size (3.4 ± 0.9 nm, Figure S11) were tested in absence of the support. This experiment constitutes a negative control. Expectedly, no conversion was detected (entry 12) which emphasizes that the AuNPs are unstable under these operating conditions. Thus, confirming the necessity to stabilize them inside of the MOF. AuNPs have reported high activity for the conversion of nitroarenes, it is necessary to colloidally stabilize the AuNPs *via* surface functionalization.[65] Otherwise, AuNPs would be aggregated, and even further, they could degrade under these aggressive catalytic conditions (*i.e.* $NaBH_4$, and organic solvent), losing their activity towards this reaction.[47]

In an attempt to extend this methodology, the reduction was tested on various molecules bearing nitro groups (Scheme 1). The choice was not arbitrary, as both molecules with electron-donating and electron-accepting groups were selected. A clear example is the conversion of nitrophenol to aminophenol with excellent yields, which could be isolated entirely and easily without byproducts (**2b**), reaching a yield of 99%. The same applies to the obtention of 1,4-diaminobenzene (**2c**), with a yield of 92%. An interesting case is the formation of 4-bromoaniline (**2d**) reaching a yield of 81%, where the halogen is a functionality susceptible to reduction. However, bromine was not affected by the reaction conditions, allowing the selective reduction of -NO_2 to -NH_2,. Finally, the reduction of the precursor dimethyl 2-nitro terephthalate (**2e**) to obtain its amino derivative (obtained with a yield of 89%) reflects that the reduction of this group can be carried out in presence of

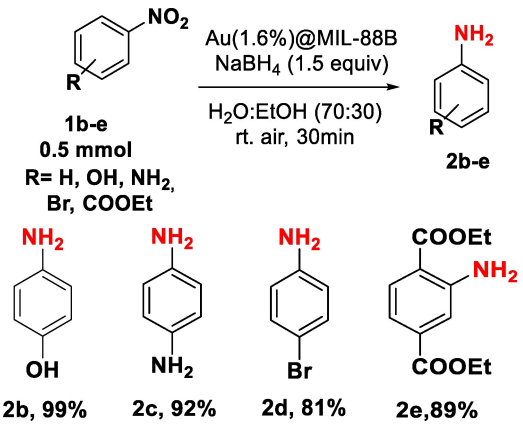

Scheme 1. Scope of reduction for nitroarenes. *Isolated yields.

other groups susceptible to be reduced and hydrolyzed (*i.e.* ester), without affecting them. This is crucial in organic synthesis, as the reduction is selective to the -NO_2 functional group.

Considering these encouraging results, the recyclability of the AuNP/MIL-88B-NH_2 catalyst was studied for the hydrogenation of nitroaniline without regeneration of the catalyst. Interestingly, the high catalytic activity of the composite was preserved after five cycles, observing a slight decrease in the 5th cycle (Figure 3). The reduction in reaction conversion may be partially attributed to a progressive mass loss of the catalyst following each material recovery process (separation by centrifugation). Nevertheless, it seems as though the decrease

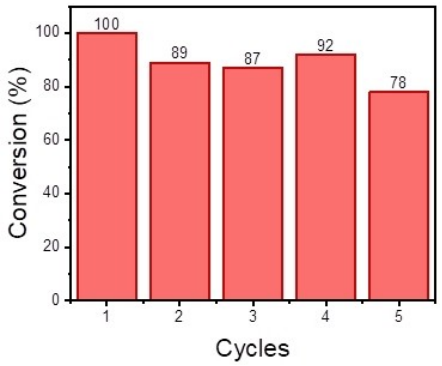

Figure 3. Recyclability test of the composite for hydrogenation of nitrobenzene to aniline.

in conversion yield after 5 cycles cannot simply be explained by material loss through recovery process. Since the AuNPs are the catalytically active component, one can suggest that the conversion yield decrease may be caused by a change in the AuNP. The change could potentially occur via Ostwald ripening in the buried NP and sintering on the surface located ones.[66] Furthermore, only a small amount of the linker was released (3.87%) after the catalysis and the crystalline structure of the MOF was confirmed by PXRD, although some changes can be observed that could be attributed to the formation of some defects (Figure S12).

Green Metrics

In order to assess the reduction of nitrophenol with regard to the 12 principles of green chemistry (P1-P12), a semi-quantitative method was first applied: the green star (see Table S3).[14] Figure 4 shows the results for an ideal green catalyst which does not require $NaBH_4$ to achieve a high conversion yield (A); our composite without using $NaBH_4$ (B, very low conversion yield); the composite under the optimized conditions using $NaBH_4$ (C); and, lastly, the recently reported AuNP/MIL-101(Fe)-NH_2 composite using $NaBH_4$, for comparison (D).[41]

The ideal catalyst reaches the greenest score in all categories. On the one hand, our composite and the reported AuNP/MIL-101(Fe)-NH_2 obtain the same scores in all categories.[41] Both materials reach the highest scores in all categories except in atom economy (P2), less hazardous chemical synthesis (P3) and inherently safer chemistry for accident prevention (P12). These lower scores are due to the excess of $NaBH_4$ and its corrosive nature. On the other hand, our composite without using $NaBH_4$ shows a green star very close to that one of the ideal catalyst, only P2 does not reach the highest score (due to the lower conversion yield). Nevertheless, it is important to consider that the green star is a semi-quantitative method which focuses on how green a process is and not how efficient or wasteful the process is. Thus, it gives a limited view of the process. Indeed, when comparing our material to recently reported NP@MOF composites, all can be described with the same green star. Therefore, mass metrics

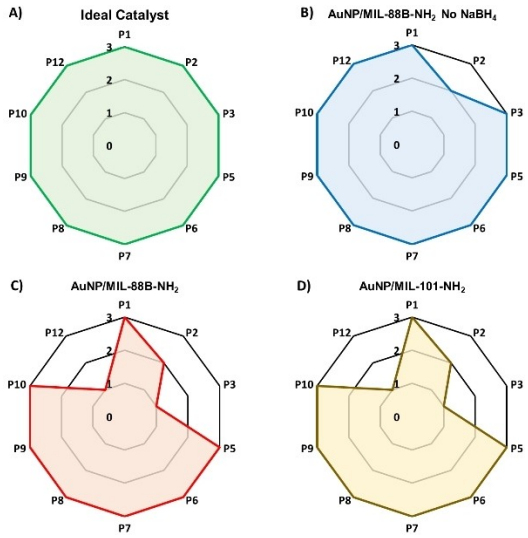

Figure 4. Green star for the reduction of nitrophenol of A) the ideal catalyst (reaching high conversion with no sacrificial agent like $NaBH_4$); B) the AuNP/MIL-88B-NH_2 composite without using $NaBH_4$; C) the AuNP/MIL-88B-NH_2 composite (optimized conditions with $NaBH_4$) and D) the reported AuNP/MIL-101-NH_2 composite (using $NaBH_4$).

were used to take the analysis a step further, using the metrics described in Table S4: the atom utilization (AU) is the mass of desired product over all products as a percentage; the E factor (E) is the ratio of waste to product; the mass intensity (MI) is the total mass over that of product; and the reaction mass efficiency (RME) is the product over the total of reactants as a percentage.[67] Using these metrics (Table S5), it becomes obvious that our AuNP/MIL-88B-NH_2 composite without $NaBH_4$ is not green. The method is wasteful (high E = 4.8 and MI = 6.1), and not efficient (low AU = 20.5% and RME = 16.4%). Furthermore, AuNP/MIL-88B-NH_2 (optimized conditions with $NaBH_4$) and the reported AuNP/MIL-101-NH_2 composite (using $NaBH_4$) can be better differentiated by comparison with the ideal catalyst. First, both AuNP/MIL-88B-NH_2 and AuNP/MIL-101-NH_2 very high efficiencies, identical to the ideal catalyst (AU = 92.2%). Further considering the efficiency with the RME, our composite reaches 63.6% (near to the ideal catalyst, 74.9%), while the reported AuNP/MIL-101-NH_2 achieves only 29.5%. This means that our composite performs particularly well whilst minimizing waste. Indeed, the waste-assessing metrics values of AuNP/MIL-88B-NH_2 are very close to the ideal catalyst (E = 0.2, MI = 1.6 *vs.* E = 0, MI = 1.3, respectively); whereas the reported AuNP/MIL-101(Fe)-NH_2 composite presents higher values in these factor (E = 2.1 and MI = 3.4) due to the high excess of $NaBH_4$. Therefore, the AuNP/MIL-88B-NH_2 composite can be seen as a promising candidate for the green catalysis of nitroarenes hydrogenation.

One-Pot Synthesis and Catalysis Experiment

With a focus on real life application, a one-pot synthesis and catalysis experiment were investigated as a proof of concept.

Indeed, for large scale industrial manufacturing, one-pot methods are favored because they are financially efficient, and require less handling and specific equipment.[68,69] As such, in the one-pot synthesis and catalysis, the MOF was first impregnated with the gold solution as in the prior experiment and then, the substrate the $NaBH_4$ were added. The composite was successfully prepared, although a slight detrimental effect on the MOF crystallinity can be observed (see PXRD and TEM; Figure S13 and S14). The AuNPs are here slightly bigger with a broader size distribution (5.7 ± 2.9 *vs.* 2.7 ± 0.9 nm-diameter; Figure S14D), indicating a lower control on the final size of the AuNPs. A similar content of small AuNPs were formed within the MOF (2.5 *vs.* 1.6% Au in the one-pot and previous composites, respectively; Figure S15). The conversion of nitroaniline occurs as well using this method with however, lower rates due to the higher heterogeneity in size of the AuNP (Table S6). The small AuNPs play a pivotal role in catalyzing the hydrogenation of nitrobenzene. In the sequence of events, the critical step for catalysis lies in the formation of the AuNP active phase. Another crucial factor is the competition by the reducing agent between the AuNPs formation and the hydrogenation catalysis. Given that these phenomena can coincide, conversion efficiency of products could be affected, as evidenced by the reduction from an initial 88 to 68% of conversion. Nevertheless, these results are encouraging, as *in situ* reactions pose a significant challenge in modern chemistry and are a focal point of interest in developing new methodologies.[69] Thus, the harmonious compatibility of two reactions is here demonstrated: the reduction of gold salts to obtain metallic NPs and the hydrogenation reaction of nitroarenes, achieving remarkable conversions.

Conclusions

A rapid, simple and highly reproducible method for the controlled formation AuNPs inside of the nanometric MIL-88B-NH_2 was successfully developed, keeping intact the nanoMOF structure while allowing the homogenous growth of AuNPs with sizes around 2.7 nm.

The potential of the resulting nanocomposite as green catalyst was studied on the valorization of the environmentally toxic nitroarenes into anilines compounds, with great value as chemical precursors and other industrial processes. The nanocomposite shows a very high conversion yield under environmentally friendly operation conditions, for different nitrobenzenes. The catalyst, operating mainly in water, proved to be environmentally friendly and cost efficient (minimizing waste), whilst still achieving high conversion rate and selectivity. Furthermore, optimized catalytic conditions are well aligned with the principles of green chemistry. The methodology used focuses on minimizing waste whilst maximizing conversion yield. Finally, with the prospect of the material being used in industrial processes a one pot synthesis and catalysis experiment was performed. The promising preliminary results (high conversion and synthesis of the composite in one step) should still be optimized and scaled up. Nevertheless, these results open up an alley towards a simple, cost efficient, reproducible, and implementable synthesis of a biosafe nanocomposite for the catalysis of anthropogenic water pollutants.

Experimental Section

Reagents

All reagents were used without further purification. $FeCl_3$ $6H_2O$ (97% purity) was purchased from Alfa Aesar, 2 aminoterephthalic acid (99%) from Thermo Fischer scientific, absolute ethanol (99% +) from VWR, acetonitrile HPLC grade and methanol HPLC grade from Serviquimia, $NaBH_4$ (95%) from TCI, Na_2HPO_4 (98%), NaH_2PO_4 (98%), nitrobenzene 99% extra pure from Thermo Fisher 4-nitroaniline 99% from Acros Organics, 4-nitrophenol 99%, 1-bromo-4-nitrobenzene 99%, diethyl 2-nitroterephtalate 99% from Sigma-Aldrich and orthophosphoric acid (85%) from Labkem. Lastly, $HAuCl_4 \cdot 3H_2O$ (99.9% +) was purchased from Sigma Aldrich.

Characterization

Powder X-ray diffraction (PXRD) patterns were acquired using a Panalytical diffractometer Empyrean DY662, in Bragg Brentano geometry from 3 to 50 (2θ). For inductively coupled plasma optical emission spectroscopy (ICP-OES) measurements the OPTIMA 7300-DV was used. SDT Q600 from TA instruments was used to carry out thermogravimetric analyses (TGA). Fourier transform infrared (FT-IR) spectra were obtained with Thermo Fisher scientific FTIR spectrometer Nicolet 6700 in attenuated total reflectance (ATR). Ultraviolet-visible (UV-VIS) spectra were collected with a UV/Vis/NIR Lambda 1050 spectrometer from Perkin Elmer. The hydrodynamic size and surface charge were measured using a nanosizer/zetasizer Nano series Nano-ZS from Malvern Instruments. The solids were dispersed in the liquid media at a concentration of 0.1 $mg \cdot mL^{-1}$ using an ultrasound tip (UP400S, Hilscher, Teltow, Germany) at 20% amplitude for 20 s. Transmission electron Microscopy (TEM) was first performed with JEOL JEM 1400 working at 120 kV. Further high angle angular dark field (HAADF) scanning transmission electron microscopy (STEM) characterizations were performed using a FEI Titan microscopy operating at 300 kV with a screen current of 50 pA. EDX images were collected with a Super-X detector with a 20 min exposure. A 3D volume was acquired for MIL-88-NH_2 using electron tomography. A tilt series was collected in the angular range of $\pm 70°$ in steps of 2° using fast tomography.[70] Reconstructions were performed using expectation maximization implemented using the ASTRA tomography toolbox[71,72] on MATLAB. Visualization of the 3D volume render were performed using Amira. Nuclear magnetic resonance (NMR) ^1H, and ^{13}C NMR and were recorded at 400 and 101 MHz respectively on a Bruker 400 spectrometer with $CDCl_3$ as a solvent. All spectra were reported in d (ppm) relative to residual solvent signal (dH ($CHCl_3$) $^1/_4$ 7.26 ppm). Gas Chromatography-Mass Spectrometry was performed using Agilent 8860 GC-5977B GC/MSD equipped with a HP5-MS UI column 30 m×0.25 mm×0.25 mm

A reverse phase High performance liquid chromatography (HPLC) Jasco LC-4000 series system, with a photo diode array (PDA) detector MD-4015 and a multisampler AS-4150 controlled by ChromNav software (Jasco Inc, Japan) was used for the quantification of the MOF degradation via the release of the constitutive linker. After centrifugation of the materials' colloidal dispersion (upon the composite formation or the catalytic reactions), the supernatant was collected, filtered (0.2 μm) and injected in the HPLC to detect the quantity of linker released in the solvent, by

using a calibration curve of the linker. The following conditions were used through a Sunfire reverse phase column (C18, 5 μm, 4.6×150 mm, Análisis Vínicos, Spain) with a flow rate of 1 mL·min^{-1} at 25 °C, using 30 μL as injection volume with a total acquisition time of 10 min, a mobile phase of phosphate buffer solution (PBS; 0.04 M, pH = 2.5): MeOH (50:50), and a retention time of 3 min and 228 nm of maximum absorbance.

Method

Synthesis:MIL-88B-NH_2 [49]

The MOF was synthesized using a reported solvothermal route with only slight modifications. In a typical synthesis, 3.33 g of 2-aminoterephthalic acid (NH_2-H_2BDC; 18.4 mmol) was solubilized in 40 mL of absolute EtOH in a 100 mL round bottom flask at 50 °C for 10 min under magnetic stirring (≈500 rpm). After that, 9.95 g of $FeCl_3 \cdot 6H_2O$ (36.8 mmol) was added along with 10 mL of absolute EtOH. The mixture was heated at 85 °C under reflux and stirring. Then, the material was recovered by centrifugation (10000 rpm for 10 min) and washed 3 times with absolute EtOH.

AuNP/MIL-88B-NH_2

Several conditions were tested for the *in situ* growth of AuNPs inside the MOF (See Table S1). The optimized synthesis conditions are as follows: 60 mg of MIL-88B-NH_2 (0.08 mmol) were dispersed in 10 mL of a MilliQ water-based solution of the gold precursor ($HAuCl_4$) at a concentration of 10 mM (0.1 mmol), being the ratio MOF/Au = 0.78. The material was left stirring for 4 h at room temperature to favor the diffusion of gold ions inside of the MOFs porosity. Then, the solution was centrifuged at 10000 rpm for 10 min, and washed twice with water to remove the excess of gold. The material was then redispersed in 10 mL of water and 2.4 mL of $NaBH_4$ 10 mM in methanol were added dropwise, while stirring (400 rpm). After complete addition of $NaBH_4$, the solution was left stirring for 10 min. The material was centrifuged at 10000 rpm for 10 min and purified by three washings with ethanol. The material was dried at a 100 °C for 4 h, the obtained yield calculated over several batches is 92 ± 5 %.

AuNPs Synthesis[73]

1 mL of sodium borohydride (17 mM) was added using a pipette to 20 mL of a 0.5 M $HAuCl_4$ solution at 100 °C. After 20 minutes, the flask was cooled to room temperature (27 °C) using a water bath.

Catalytic Reaction Tests

The reactions were carried out in a 10 mL glass vial, equipped with a cap and a magnetic stirrer. Nitrocompounds (0.5 mmol), $NaBH_4$ as hydrogen source (0.075 mmol) and 10 mg of Au/MIL-88B-NH_2 as catalyst were dissolved in 2 mL of reaction mixture and stirred under air atmosphere for 1 h. Then, the reaction crude was placed into a separatory funnel and necessary amounts of ethyl acetate and water were added. The organic layer was separated. The combined organic extract was dried over anhydrous Na_2SO_4. Finally, the product was isolated by column chromatography (silica gel, eluent: 8:2 hexane/ethyl acetate). The compounds were purified by flash column and the identity of all the products was confirmed by ^{1}H and ^{13}C NMR.

One-Pot Synthesis and Catalysis Experiment

10 mg of MIL-88B-NH_2 (0.08 mmol) were dispersed in a 1.6 mL MilliQ water-based solution of $HAuCl_4$ at a concentration of 10 mM (0.1 mmol). The material was left stirring for 4 h at room temperature to favor the diffusion of gold ions inside of the MOF porosity. Then, the solution was centrifuged at 10000 rpm for 10 min, and washed twice to remove the excess of gold. The material was then redispersed, along with 69 mg of nitrobenzene, in 2.1 mL of water and 0.9 mL of methanol. Finally, 60 mg of $NaBH_4$ were added, while under stirring (400 rpm). The solution was left stirring for 10 min and the material was centrifuged at 10000 rpm for 10 min and washed thrice with ethanol.

Supporting Information

The authors have cited additional references within the Supporting Information.

Acknowledgements

The authors gratefully acknowledge the European Union's Horizon 2020 research and innovation program under the Marie Skłodowska-Curie Grant ID: 860942 (HeatNMof ITN).

Conflict of Interests

The authors declare no conflict of interest.

Data Availability Statement

The data that support the findings of this study are available from the corresponding author upon reasonable request.

Keywords: Metal organic frameworks · Gold nanoparticles · Nanocomposites · Green catalysis · Hydrogenation

[1] X. Peng, L. Chen, Y. Li, *J. Mol. Catal.* **2022**, *529*, 112568.
[2] S. Witzel, A. S. K. Hashmi, J. Xie, *Chem. Rev.* **2021**, *121*, 8868–8925.
[3] C. Busco, M. L. Frigo, A. Riccaboni, P. Quattrone, *Integr. Report. Concepts Cases that Redefine Corp. Account.* **2013**, 1–350.
[4] R. Goodland, *Sustainability* **2017**, *26*, 251–274.
[5] A. Sharma, G. Singh, A. O'Donovan, M. Sharma, A. Kaur, S. Kumar Arya, *Fuel* **2023**, *350*, 128837.
[6] A. Kate, L. K. Sahu, J. Pandey, M. Mishra, P. K. Sharma, *Curr. Res. Green Sustain. Chem.* **2022**, *5*, 100248.
[7] R. Zheng, Z. Liu, Y. Wang, Z. Xie, M. He, *Joule* **2022**, *6*, 1148–1159.
[8] S. Li, Y. Wu, M. U. Dao, E. N. Dragoi, C. Xia, *Chemosphere* **2023**, *318*, 137954.
[9] J. Liu, *Curr. Opin. Green Sustain. Chem.* **2020**, *22*, 54–64.
[10] Y. Kim, C. J. Li, *Green Synth. Catal.* **2020**, *1*, 1–11.
[11] T. C. Ho, *Catal. Rev.* **1988**, *30*, 117–160.
[12] K. Pobłocki, J. Drzeżdżon, B. Gawdzik, D. Jacewicz, *Green Chem.* **2022**, *24*, 9402–9427.
[13] A. A. Rico-Barragán, J. Raziel Álvarez, E. Hernández-Fernández, J. Rodríguez-Hernández, M. A. Garza-Navarro, N. E. Dávila-Guzmán, *Polyhedron* **2022**, *225*, DOI 10.1016/j.poly.2022.116052.
[14] M. G. T. C. Ribeiro, D. A. Costa, A. A. S. C. Machado, *Green Chem. Lett. Rev.* **2010**, *3*, 149–159.

[15] J. C. G. Sousa, A. R. Ribeiro, M. O. Barbosa, M. F. R. Pereira, A. M. T. Silva, *J. Hazard. Mater.* **2018**, *344*, 146–162.
[16] S. E. J. B. Halling-Sorensen, *Stud. Environ. Sci.* **1993**, *54*, 3–40.
[17] J. Tiwari, P. Tarale, S. Sivanesan, A. Bafana, *Environ. Sci. Pollut. Res. Int.* **2019**, *26*, 28650–28667.
[18] R. Begum, R. Rehan, Z. H. Farooqi, Z. Butt, S. Ashraf, *J. Nanopart. Res.* **2016**, *18*, DOI 10.1007/s11051-016-3536-5.
[19] M. Orlandi, D. Brenna, R. Harms, S. Jost, M. Benaglia, *Org. Process Res. Dev.* **2018**, *22*, 430–445.
[20] M. Anjalin, N. Kanagathara, A. R. Baby Suganthi, *Mater. Today: Proc.* **2020**, *33*, 4751–4755.
[21] P. Zhao, X. Feng, D. Huang, G. Yang, D. Astruc, *Coord. Chem. Rev.* **2015**, *287*, 114–136.
[22] P. C. Nagajyoti, K. D. Lee, T. V. M. Sreekanth, *Environ. Chem. Lett.* **2010**, *8*, 199–216.
[23] K. S. Egorova, V. P. Ananikov, *Organometallics* **2017**, *36*, 4071–4090.
[24] V. C. Thipe, A. R. Karikachery, P. Çakılkaya, U. Farooq, H. H. Genedy, N. Kaeokhamloed, D. H. Phan, R. Rezwan, G. Tezcan, E. Roger, K. V. Katti, *J. Drug Delivery Sci. Technol.* **2022**, *70*, 103256.
[25] K. Liu, R. Qin, N. Zheng, *J. Am. Chem. Soc.* **2021**, *143*, 4483–4499.
[26] M. Muzzio, J. Li, Z. Yin, I. M. Delahunty, J. Xie, S. Sun, *Nanoscale* **2019**, *11*, 18946–18967.
[27] C. M. Hendrich, K. Sekine, T. Koshikawa, K. Tanaka, A. S. K. Hashmi, *Chem. Rev.* **2021**, *121*, 9113–9163.
[28] N. Sarfraz, I. Khan, *Chem. Asian J.* **2021**, *16*, 720–742.
[29] H. T. Phan, A. J. Haes, *J. Phys. Chem. C* **2019**, *123*, 16495–16507.
[30] A. Corma, H. Garci, *Chem. Soc. Rev.* **2008**, *37*, 2096–2126.
[31] M. K. Corbierre, N. S. Cameron, M. Sutton, S. G. J. Mochrie, L. B. Lurio, A. Rühm, R. B. Lennox, *J. Am. Chem. Soc.* **2001**, *123*, 10411–10412.
[32] A. Dhakshinamoorthy, A. M. Asiri, H. Garcia, *ACS Catal.* **2017**, *7*, 2896–2919.
[33] Y. Shan, G. Zhang, Y. Shi, H. Pang, *Cell Reports Phys. Sci.* **2023**, *4*, 101301.
[34] D. Li, H. Q. Xu, L. Jiao, H. L. Jiang, *EnergyChem* **2019**, *1*, 100005.
[35] C. Wu, X. Zhao, D. Wang, X. Si, T. Li, *Chem. Sci.* **2022**, *13*, 13338–13346.
[36] F. Ke, J. Zhu, L. G. Qiu, X. Jiang, *Chem. Commun.* **2013**, *49*, 1267–1269.
[37] J. Qiu, L. Yang, M. Li, J. Yao, *Mater. Res. Bull.* **2019**, *112*, 297–306.
[38] J. S. Wang, F. Z. Jin, H. C. Ma, X. B. Li, M. Y. Liu, J. L. Kan, G. J. Chen, Y. Bin Dong, *Inorg. Chem.* **2016**, *55*, 6685–6691.
[39] X. Cai, Z. Xie, D. Li, M. Kassymova, S. Q. Zang, H. L. Jiang, *Coord. Chem. Rev.* **2020**, *417*, 213366.
[40] Y. Zhong, P. Liao, J. Kang, Q. Liu, S. Wang, S. Li, X. Liu, G. Li, *J. Am. Chem. Soc.* **2023**, *145*, 4659–4666.
[41] C. Hu, C. Yang, X. Wang, X. Wang, S. Zhen, L. Zhan, C. Huang, Y. Li, *Sep. Purif. Technol.* **2022**, *300*, 121801.
[42] P. Horcajada, H. Chevreau, D. Heurtaux, F. Benyettou, F. Salles, T. Devic, A. Garcia-Marquez, C. Yu, H. Lavrard, C. L. Dutson, E. Magnier, G. Maurin, E. Elkaïm, C. Serre, *Chem. Commun.* **2014**, *50*, 6872–6874.
[43] C. Tamames-Tabar, D. Cunha, E. Imbuluzqueta, F. Ragon, C. Serre, M. J. Blanco-Prieto, P. Horcajada, *J. Mater. Chem. B* **2014**, *2*, 262–271.
[44] P. Horcajada, F. Salles, S. Wuttke, T. Devic, D. Heurtaux, G. Maurin, A. Vimont, M. Daturi, O. David, E. Magnier, N. Stock, Y. Filinchuk, D. Popov, C. Riekel, G. Férey, C. Serre, *J. Am. Chem. Soc.* **2011**, *133*, 17839–17847.
[45] E. L. First, C. A. Floudas, *Microporous Mesoporous Mater.* **2013**, *165*, 32–39.
[46] G. Zheng, I. Pastoriza-Santos, J. Pérez-Juste, L. M. Liz-Marzán, *SmartMat* **2021**, *2*, 446–465.
[47] Y. Mikami, A. Dhakshinamoorthy, M. Alvaro, H. García, *Catal. Sci. Technol.* **2013**, *3*, 58–69.
[48] X. Li, Y. Zhang, G. K. Liu, Z. Luo, L. Zhou, Y. Xue, M. Liu, *RSC Adv.* **2022**, *12*, 7635–7651.
[49] S. Bauer, C. Serre, T. Devic, P. Horcajada, J. Marrot, G. Férey, N. Stock, *Inorg. Chem.* **2008**, *47*, 7568–7576.
[50] C. F. Holder, R. E. Schaak, *ACS Nano* **2019**, *13*, 7359–7365.
[51] R. Rotaru, M. Savin, N. Tudorachi, C. Peptu, P. Samoila, L. Sacarescu, V. Harabagiu, *Polym. Chem.* **2018**, *9*, 860–868.
[52] P. Horcajada, F. Salles, S. Wuttke, T. Devic, D. Heurtaux, G. Maurin, A. Vimont, M. Daturi, O. David, E. Magnier, N. Stock, Y. Filinchuk, D. Popov, C. Riekel, C. Serre, *J. Am. Chem. Soc.* **2011**, *133*, 17839–17847.
[53] K. I. Hadjiivanov, D. A. Panayotov, M. Y. Mihaylov, E. Z. Ivanova, K. K. Chakarova, S. M. Andonova, N. L. Drenchev, *Chem. Rev.* **2021**, *121*, 1286–1424.
[54] M. H. Pham, G. T. Vuong, A. T. Vu, T. O. Do, *Langmuir* **2011**, *27*, 15261–15267.
[55] J. H. Yoon, J. S. Park, S. Yoon, *Langmuir* **2009**, *25*, 12475–12480.
[56] S. Bhattacharjee, *J. Controlled Release* **2016**, *235*, 337–351.
[57] J. Turkevich, *Gold Bull.* **1995**, *18*, 125–131.
[58] J. Turkevich, P. C. Stevenson, *Discuss. Faraday Soc.* **1951**, *11*, 55–75.
[59] L. M. Liz-Marzán, *Langmuir* **2006**, *22*, 32–41.
[60] J. W. Park, J. S. Shumaker-Parry, *J. Am. Chem. Soc.* **2014**, *136*, 1907–1921.
[61] F. J. Flórez Barajas, Z. C. Sánchez Acevedo, H. Peña Pedraza, *Respuestas* **2019**, *24*, 49–55.
[62] V. A. Dhumale, R. K. Gangwar, S. S. Datar, R. B. Sharma, *Mater. Express* **2012**, *2*, 311–318.
[63] L. Pauling, S. B. Hendricks, *J. Am. Chem. Soc.* **1925**, *47*, 781–790.
[64] B. Werbel, J. H. Saylor, P. M. Gross, *J. Am. Chem. Soc.* **1941**, *63*, 1346–1347.
[65] C. Torres, C. Campos, J. L. G. Fierro, M. Oportus, P. Reyes, *Catal. Lett.* **2013**, *143*, 763–771.
[66] C. J. Gommes, *Nanoscale* **2019**, *11*, 7386–7393.
[67] J. Martínez, J. F. Cortés, R. Miranda, *Processes* **2022**, *10*, 1274.
[68] T. Bieringer, S. Buchholz, N. Kockmann, *Chem. Eng. Technol.* **2013**, *36*, 900–910.
[69] C. Holtze, R. Boehling, *Curr. Opin. Chem. Eng.* **2022**, *36*, 100798.
[70] H. Vanrompay, A. Skorikov, E. Bladt, A. Béché, B. Freitag, J. Verbeeck, S. Bals, *Ultramicroscopy* **2021**, *221*, 113191.
[71] W. van Aarle, W. J. Palenstijn, J. De Beenhouwer, T. Altantzis, S. Bals, K. J. Batenburg, J. Sijbers, *Ultramicroscopy* **2015**, *157*, 35–47.
[72] W. van Aarle, W. J. Palenstijn, J. Cant, E. Janssens, F. Bleichrodt, A. Dabravolski, J. De Beenhouwer, K. Joost Batenburg, J. Sijbers, *Opt. Express* **2016**, *24*, 25129.
[73] A. C. Lucioni, *Rev. Soc. Quim. Peru* **2012**, *78*, 79–90.

Manuscript received: January 31, 2024
Accepted manuscript online: March 21, 2024
Version of record online: ■■, ■■

RESEARCH ARTICLE

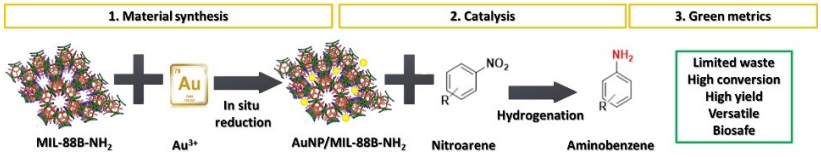

This work presents the *in situ* formation of small gold nanoparticles inside the iron carboxylate metal organic framework MIL-88B-NH_2. The resulting nanocomposite was tested in the hydrogenation of diverse nitroarenes, reaching high conversion rates in a sustainable reaction, as proven by green metrics.

*S. N. K. Lelouche, Dr. I. Lemir, Dr. C. Biglione, T. Craig, Prof. S. Bals, Dr. P. Horcajada**

1 – 10

AuNP/MIL-88B-NH_2 Nanocomposite for the Valorization of Nitroarene by Green Catalytic Hydrogenation